14th Australasian Fluid Mechanics Conference
Adelaide University, Adelaide, Australia
10-14 December 2001

Quantification of Mixing Characteristics for the Optimisation of Combustion in Rotary Kilns

Jordan J. Parham[1], Graham J. Nathan and Zeyad T. Alwahabi

Department of Mechanical Engineering
University of Adelaide, Adelaide, South Australia, 5005 AUSTRALIA

[1]Current address: School of Mechanical Engineering
University of Edinburgh, Edinburgh, Scotland, EH9 3JL UNITED KINGDOM

Abstract

A planar laser-induced fluorescence technique is used to study the mixing characteristics from a controllable, fixed geometry, precessing jet nozzle. Measurements are made to quantify the change in mean and fluctuating centreline conserved scalar concentration, probability distribution function and jet spread as a function of the momentum fraction of an axial shaping jet to precessing jet flows. The results are compared with previous small and large-scale combustion measurements and indicate that the mixing and combustion characteristics are well correlated by the momentum fraction. Hence the preferred scalar mixing characteristics associated with low NO_x emissions and high radiant heat transfer for rotary kiln burner designs are identified.

Introduction

It is well known that the mixing characteristics associated with a particular gas-fired burner design can significantly influence its combustion performance. However, a quantitative understanding of what aspects of mixing are most significant or how different mixing characteristics correlate with pollutant emissions and heat transfer, is yet to be developed. Such understanding is advantageous in developing effective designs and in the control of combustion systems. Furthermore, most studies of the mixing characteristics of practical burner systems (e.g. swirl and bluff body burners) have been performed using velocity measurements rather than scalar concentration measurements. For example, Chen *et al.* [1] used velocity measurements to demonstrate that flame properties from a swirl burner can be altered by controlling the vortex strength of the swirling flow and fuel jet momentum. A momentum ratio based similarity parameter which is applicable to flows from swirl and bluff-body nozzles was thus derived. Limited scalar concentration measurements on a bluff-body nozzle, have been made by Namazian *et al.* [10]. More extensive conserved scalar concentration measurements in bluff-body flames were made by Dally *et al.* [3], who also measured the concentration of reacting gas species. Distinctive changes in the mean and fluctuating components of concentration and probability distribution functions were demonstrated for different momentum ratios by both researchers. However, there is little correlation between these changes and emission characteristics and no correlation with heat transfer properties. Furthermore, bluff-body burners have limited industrial application.

The present investigation considers mixing and combustion within rotary kilns, such as are found in the cement, lime and alumina industries. Unlike boilers, swirl burner designs are generally not applicable to rotary kiln installations due to differences in confinement, geometric configuration and different heat release profile requirements. Hence the low NO_x emission features developed for swirl burners cannot be used in rotary kilns. On the other hand, Precessing Jet (PJ) nozzles, based on the design shown in Figure 1, are mechanically simple and are suitable for application in rotary kilns. In gas-fired kilns they have been found to reduce NO_x emissions by 40 to 70% [7,8] and to increase flame radiation relative to conventional burner flames [11,12]. Nathan *et al.* [13] gives an extensive description of the PJ flow and the conditions under which it arises.

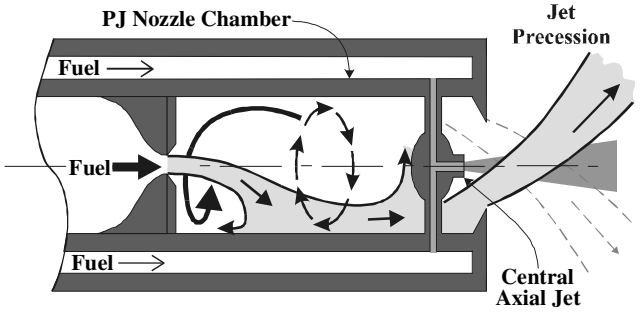

Figure 1 : Schematic diagram of the fluidic Precessing Jet (PJ) nozzle with a central axial jet (CAJ) for flame shaping.

A secondary fuel jet, here termed a Central Axial Jet (CAJ) has been developed to control the mixing and hence combustion characteristics of the flame (Figure 1). Controlling the ratio of the two flows provides control of the mixing without the need to move internal components. Parham *et al.* [14] and Parham [17] have shown that a broad range of mixing characteristics can be generated by the PJ-CAJ nozzle, from those typical of a precessing jet flow to those typical of a simple jet flow. Parham [17] has demonstrated that the control of flow characteristics can be correlated with the fraction of CAJ momentum to combined jet momentum, $\Gamma_{CAJ} = G_{CAJ}/(G_{CA} + G_{PJ})$. Note that the PJ nozzle momentum is calculated here at the upstream orifice because of the complexity of the flow at the exit plane of the nozzle. In practice Γ_{CAJ} is varied by altering the relative flowrates through the CAJ and PJ nozzles.

Flow visualisation experiments [14,17] have demonstrated that, for momentum fractions in the range $0 \le \Gamma_{CAJ} \le 0.2$, the combined PJ and CAJ flow field has many characteristics similar to the precessing jet flow on its own. Hence this class of flow field is described as "precessing jet dominated". For momentum fractions in the range $0.23 \le \Gamma_{CAJ} \le 1$, the combined flow is dominated by the features of the central axial jet. Pilot-scale combustion experiments undertaken by Parham *et al.* [15] have demonstrated that the flame characteristics of a confined PJ nozzle can also be correlated with Γ_{CAJ}. Increasing Γ_{CAJ} from 0 to 0.32 moves the peak heat flux further down the kiln by approximately one kiln diameter and also broadens the profile so that the peak heat flux is slightly reduced. The highest total heat flux recorded is associated with flames with $\Gamma_{CAJ} = 0.11 - 0.25$, consistent with unconfined flame measurements undertaken by Parham [17]. These measurements also show that the NO_x

emissions are minimised within the same range of momentum fractions, consistent with the results obtained in full-scale industrial kilns [5].

Combined PJ and CAJ flows are therefore not only a highly relevant flow, but they provide a tool for creating a range of different turbulent flow characteristics which are associated with different characteristics of radiant heat transfer, flame shape and emissions. Whilst the optimal operating range of the PJ-CAJ nozzle for maximum heat transfer and minimum emissions has been determined from combustion experiments, the mixing characteristics associated with this range of conditions have not. Therefore the aim of the present study is to explore the range of scalar mixing characteristics generated by the PJ-CAJ nozzle, with a view to identifying the mixing characteristics associated with the optimal combustion performance for rotary kiln applications.

Experimental Method

The combined jets from a PJ and CAJ nozzle were investigated within a confining tube in a water tunnel to provide a uniform co-flow (Figure 2). The geometric ratio of the nozzle diameter to that of the confining tube was chosen to represent that of a rotary kiln. Scaling was performed using the Thring-Newby similarity criterion following the finding of Parham [17] that this criterion is the most appropriate for the simulation of confined flows from a PJ nozzle.

Quantitative measurements of the mixing characteristics were obtained using Planar Laser-Induced Fluorescence (PLIF). A detailed description of the experimental technique and measurements is given by Parham [17] and Parham *et al.* [18]. Briefly, the jet nozzle was aligned on the axis of symmetry of a 0.5×0.5m cross-section, closed-circuit water-tunnel (Figure 2). The horizontal laser sheet from a Coherent Infinity 40-100 Nd:YAG laser was aligned through the jet axis. The laser was operated at its maximum power output of 250mJ/pulse at 532nm and a repetition rate of 6Hz. The fluorescent marker was 5(&6) carboxy-2′,7′-dichlorofluorescein at a molar concentration of 7.9×10^{-6} M. Karasso and Mungal [6] have demonstrated that this dye behaves linearly when excited by a Nd:YAG laser. The dye was stored in separate supply tanks and pumped through the respective jets at flow rates controlled by Fischer and Porter rotameters.

A Kodak MegaPlus ES1.0 camera with a Fujinon CF12.5A wide-angle lens was positioned at right angles to the laser sheet to capture the images. A long-pass filter in front of the camera lens blocked scattered light from the laser. Typically one to 4 batches of 152 images were collected for each condition.

The geometry of the PJ nozzle was fixed with an upstream orifice diameter of d_{or} = 7.5mm, a chamber diameter of d_{PJ} = 38mm and a central axial jet diameter of d_{CAJ} = 4.5mm. The design of the nozzle conforms with the optimal geometric requirements specified by Hill *et al.* [4]. The nozzle was operated at a constant total flowrate of approximately 1,400 L/hr for all Γ_{CAJ}. For PJ only flow ($\Gamma_{CAJ} = 0$) this flowrate corresponds to a Reynolds number at the upstream orifice of 66,200. Confinement around the jet was provided by a D_{duct} = 390mm internal diameter perspex duct of 5mm wall thickness mounted concentric to the nozzle axis. The water-tunnel was operated with a constant co-flow velocity of U_a = 0.06m/s. These conditions satisfy the Thring-Newby similarity criterion for isothermal similarity with the pilot-scale combustion experiments.

The experimental region of interest was approximately 504mm×508mm so that the spatial resolution is about 0.5×0.5×0.5mm. This is approximately eight times larger than the Batchelor scale and about five times larger than the Kolmogorov scale in the far field of the jet [17]. Nevertheless, the spatial resolution is comparable with that of other PLIF investigations such as Dahm and Dimotakis [2], so the accuracy of the mean jet concentration calculations is expected to be good, while the measurements of concentration fluctuations will be slightly lower than the actual values.

Suitable digital image processing was performed on each image to obtain a quantitative measurement of the jet fluid concentration. This involved correcting for background noise, laser sheet non-uniformity, camera-optics gain distribution, laser power fluctuations and absorption. The images of concentration distribution were then normalised to the concentration at the upstream orifice diameter to obtain the conserved dye concentration, ξ. Individual images were summed to calculate the spatial distribution of the mean and fluctuating components of the conserved scalar concentration. The number of images used for the calculations varied depending on the jet condition, from 152 for $\Gamma_{CAJ} = 0.11$, for example, to 1216 for $\Gamma_{CAJ} = 0$.

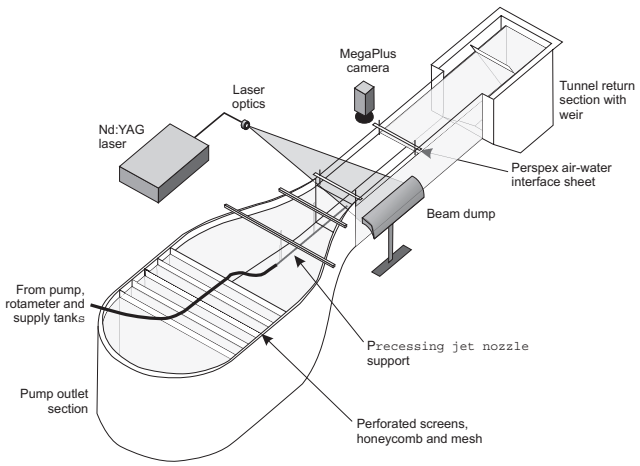

Figure 2 : Schematic diagram of the setup to investigate the mixing characteristics of the combined Central Axial Jet and Precessing Jet nozzle by quantitative PLIF.

Results

The instantaneous two-dimensional images of the conserved scalar concentration from a PJ nozzle obtained in the present experiments demonstrated the characteristic wide spreading angle and large-scale structures also observed by Nathan *et al.* [13]. Here we present only a statistical comparison of the effect of the momentum fraction, Γ_{CAJ}, on the centreline mixing characteristics, so no instantaneous images are included. However instantaneous concentration images obtained using the same facility and nozzle, but for different conditions, have been presented by Parham *et al.* [16].

Jet flows have been widely studied and are known to evolve from the initial flow defined by the jet exit through a transition region to a fully developed, self-similar region where the decay rate and spread angle are linear. Self similarity of the mean flow is found typically to occur within about ten nozzle diameters while self-similarity of the fluctuating statistics is not attained until 50 to 70 diameters, depending upon the initial conditions. These trends of a transition to a steady state are also found in the entire range of jet flows from precessing to axial jet flows, see Figure 3. However there are dramatic differences both in the initial flow

(spread and decay) and in the nature of the final asymptotic state. Note that the axial distance from the upstream orifice, x, is referenced to the upstream orifice of the PJ nozzle by subtracting the length of the nozzle chamber, L, and normalised by the upstream orifice diameter, d_{or}, which is approximately one-fifth of the chamber diameter. The central axial jet is a factor of 0.6 smaller than d_{or}.

Figure 3a shows the effect of the momentum fraction, Γ_{CAJ}, on the inverse conserved scalar concentration on the jet axis, $\overline{\xi}_{ja}$. At low values of Γ_{CAJ} the far-field rate of concentration decay is comparable for all jets, although the absolute decay at a given distance differs due to different initial decay rates. However, for $\Gamma_{CAJ} > 0.11$, the CAJ dominates the flow features and the final rate of decay tends towards that of the CAJ on its own. The concentration decay constant, K_1, is defined as the inverse of the slope of the line of best fit to the conserved scalar concentration decay profile shown in Figure 3a. The decay constant for the CAJ only condition, when normalised to the CAJ exit diameter, is $K_1 = 5.95$, which agrees well with the range reported for simple jets in the literature [9]. The $\Gamma_{CAJ} = 0.17$ case has the lowest inverse conserved scalar concentration value at a given axial position for the experiments conducted.

The effect of CAJ momentum fraction on the jet concentration half-width is illustrated in Figure 3b. As with the inverse concentration plots, two different flow regimes can be identified depending on the momentum fraction. At low Γ_{CAJ}, there is a very rapid increase in jet spread in the near-field, indicative of a PJ dominated flow, while at higher Γ_{CAJ}, the absence of the rapid rise is indicative of a CAJ dominated flow. In the far field of a jet in the PJ dominated flow regime, increasing the momentum fraction reduces the jet spreading rate, with the minimum spreading rate, K_2, occurring at $\Gamma_{CAJ} = 0.11$. Further increasing Γ_{CAJ} increases the jet spreading rate for the range of conditions investigated. Similar behaviour is also observed for the far field virtual origin, which initially moves downstream as x/d_{or} increases, until reaching a peak at $\Gamma_{CAJ} = 0.11$. Further increasing Γ_{CAJ} leads to a step change in the location of the virtual origin, which then moves upstream. The spreading rate of the CAJ only case, when normalised by the CAJ exit diameter, d_{CAJ}, is $K_2 = 0.090$, well within the range reported for simple jets, see Mi *et al.* [9].

The oscillating and rapidly spreading precessing jet flow has a dramatic influence on the near-field concentration fluctuation intensity, $\xi_{rms-ja}/\overline{\xi}_{ja}$, sometimes termed the "unmixedness", on the jet axis. Figure 3c shows that PJ dominated flows exhibit a clear peak in the normalised fluctuations about five upstream orifice diameters downstream from the exit plane. As the momentum fraction of the CAJ is increased, the magnitude of this peak diminishes until, in the CAJ dominated flow regime, it is no longer present. Increasing Γ_{CAJ} also moves the location of the peak fluctuation intensity further downstream from the nozzle exit and results in a slight decrease in the asymptotic value of the unmixedness. The asymptotic value of concentration fluctuation intensity for the CAJ on its own is 0.204, which is less than that of any of the combined CAJ and PJ flows, even for very high Γ_{CAJ} and agrees well the results obtained for other types of simple jet, see Mi *et al.* [9].

The effect of the flow regime (PJ or CAJ dominated) on the mixing from the PJ nozzle is further shown by the probability distribution of conserved scalar concentration on the jet axis, *pdf*(ξ). Figure 4 shows that as the momentum fraction is increased from $\Gamma_{CAJ} = 0$ to $\Gamma_{CAJ} = 0.17$, the distribution of scalar concentrations found in the jet far field increases. However, in the momentum fractions corresponding to the CAJ dominated regime, $\Gamma_{CAJ} > 0.23$, the range of conserved scalar concentrations is lower. Similarly the most probable scalar concentration also increases with momentum ratio and reaches a maximum at $\Gamma_{CAJ} = 0.17$, beyond which it decreases in value. This trend is more clearly observed closer to the nozzle than in the far field location of $(x-L)/d_{or} \approx 51$ used to calculate Figure 4.

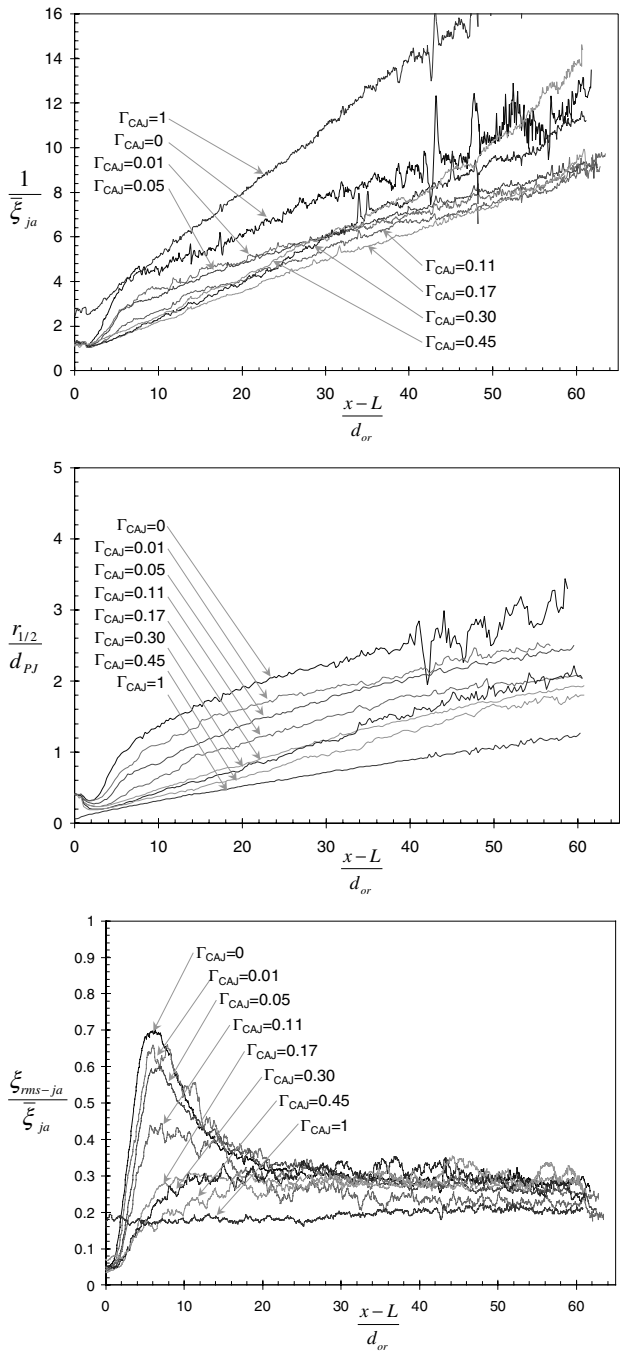

Figure 3 : The effect of momentum fraction, Γ_{CAJ}, on (a) the mean conserved scalar concentration on the jet axis, $\overline{\xi}_{ja}$, (b) the concentration half-width, $r_{1/2}/d_{PJ}$, and (c) the concentration fluctuation intensity on the jet axis, $\xi_{rms-ja}/\overline{\xi}_{ja}$. Conditions: $U_a = 0.06$m/s, $D_{duct}/d_{PJ} = 10.3$, $m_a/m_0 = 18.4$ except for $\Gamma_{CAJ} = 1$ (CAJ only, $m_a/m_0 = 122$).

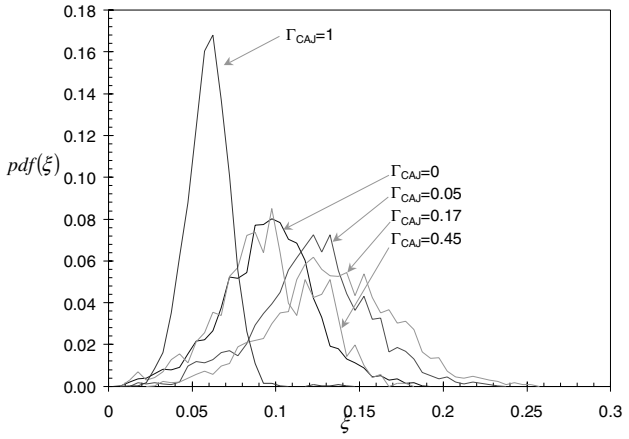

Figure 4 : The effect of momentum fraction, Γ_{CAJ}, on the probability distribution function of conserved scalar concentration on the jet axis in the far field of the PJ nozzle at $(x\text{-}L)/d_{or} \approx 51$. Conditions as for Figure 3.

Discussion

Previous measurements of combined PJ-CAJ flames have shown that the "optimal" combination of high heat transfer and low NO_x emissions occurs with $\Gamma_{CAJ} = 0.11\text{-}0.25$. For example, Parham *et al*. [15] showed that the flame associated with highest heat transfer and lowest emissions when burning natural gas in a pilot-scale rotary kiln occurs at a momentum fraction of $\Gamma_{CAJ} = 0.15$. The present measurements demonstrate that unique mixing characteristics are associated with flows within this range of momentum fractions and the optimal flame condition in particular. Figure 4 shows that a momentum fraction of $\Gamma_{CAJ} = 0.17$ is associated with the widest range of scalar concentration fluctuations and the maximum conserved scalar concentration on the jet axis. Importantly, all of the PJ dominated flows, which have better performance than the simple jet flame, also have a much wider spectrum of scalar concentration distributions. Furthermore the flow with the preferred combustion characteristics in the present environment does not have the widest initial jet spread or centreline concentration decay. This demonstrates that there is an optimal initial spreading rate and that there may be no benefit in increased jet "excitation" beyond a critical value.

Conclusion

The results of isothermal and combustion experiments on the combined precessing jet and central axial jet nozzle are consistent and demonstrate that control of the combined jet mixing and combustion characteristics is well correlated with the momentum fraction of central axial jet to the combined jet momentum, Γ_{CAJ}. The present quantitative PLIF experiments have shown that distinctive mixing characteristics are associated with the precessing jet dominated flow regime, $\Gamma_{CAJ} < 0.2$, and the CAJ dominated flow regime, $\Gamma_{CAJ} > 0.23$.

The present isothermal experiments have also identified the scalar mixing characteristics that are associated with the preferred combustion performance in a rotary kiln burner where low NO_x emissions and high radiant heat transfer are desired. This is shown to occur for a momentum fraction of $\Gamma_{CAJ} = 0.17$. At this flow condition, the measured conserved scalar concentration on the jet axis at a given point is the highest ($K_1 = 7.83$, $x_{0.1}/d_{or} = 4.82$) and the range of scalar concentrations on the jet axis is the largest of any jet from the combined jet flows investigated ($0.0275 \le \xi_c \le 0.2525$ at $(x\text{-}L)/d_{or} \approx 51$). The profile of concentration fluctuation intensity profile also does not peak close to the nozzle exit, characteristic of a CAJ dominated flow condition, but approaches the asymptotic concentration fluctuation intensity value of $\xi_{rms-ja}/\overline{\xi}_{ja} = 0.279$ more rapidly than any of the CAJ dominated flow conditions. These results provide new potential for seeking to identify preferred mixing characteristics for burner designs associated with natural gas burners which aim to generate high radiation flux and low NO_x emissions.

Acknowledgements

The assistance of Associate Professor Keith King in securing the Infinity Nd:YAG laser for use in the present experiments is most appreciated. The assistance of members of the Turbulence, Energy and Combustion group, in particular Mr. Philip Cutler, and Dr. David Nobes in helping to set up the experiments was invaluable. This research was supported by the financial assistance of Fuel and Combustion Technology Ltd. and the Australian Research Council through the Collaborative Grants Scheme.

References

[1] Chen, R.-H., Driscoll, J.F., Kelly, J., Namazian, M. and Schefer, R.W., *Combust. Sci. and Tech.,* **71**, 197-217, 1990.

[2] Dahm, W.J.A. and Dimotakis, P.E., *J. Fluid Mech.*, **21**7, 299-330, 1990.

[3] Dally, B.B., Masri, A.R., Barlow, R.S. and Fiechtner, G.J. *Combust. Flame*, **114** (1-2): 119-148, 1998.

[4] Hill, S.J., Nathan, G.J. and Luxton, R.E., *Eleventh Australasian Fluid Mechanics Conferenc*e, University of Tasmania, Hobart, Australia, 14-18 December, 1113-1116, 1992.

[5] Hill, S.J., Rapson, D.S. and Nathan, G.J., *The Australian Symposium on Combustion*, The Combustion Institute (Australia), Gawler, South Australia, November 1995.

[6] Karasso, P.S. and Mungal, M.G., *Expt. Fluid*s, **2**3, 382-387, 1997.

[7] Manias, C.G. and Nathan, G.J., *World Cement*, **24**, (3), 1993.

[8] Manias, C.G. and Nathan, G.J., *World Cement*, **25**, (5), 54-56, 1994.

[9] Mi, J., Nobes, D.S. and Nathan, G.J., *J. Fluid. Mech.*, **432**, 91-125, 2001.

[10] Namazian, M., Kelly, J. and Schefer, R.W., *AIAA Journa*l, **30** (2), 384-394, 1992.

[11] Nathan, G.J. and Luxton, R.E., *Transport Phenomena in Heat and Mass Transfer*, **2**, 1297-1307, 1992

[12] Nathan, G.J., Brumale, S., Proctor, D. and Luxton, R.E., *Combustion and Emissions Control*, The Institute of Energy, 213-230, 1993.

[13] Nathan, G.J., Hill, S.J. and Luxton, R.E., *J. Fluid Mech.*, **38**0, 347-380, 1998.

[14] Parham, J.J., Nathan, G.J. and Luxton, R.E. *Thirteenth Australasian Fluid Mechanics Conferenc*e, Monash University, Victoria, Australia, 595-598, 1998.

[15] Parham, J.J., Nathan, G.J., Smart, J.P., Hill, S.J. and Jenkins, B.G. *J. Inst. Energy*, **73** (494), 25-34, 2000.

[16] Parham, J.J., Nathan, G.J. and Alwahabi, Z.T. *The Album of Visualizatio*n, **1**7, The Visualization Society of Japan, 2000.

[17] Parham, J.J. *Ph.D. thesis*, Dept. Mech. Eng., University of Adelaide, 2000.

[18] Parham, J.J., Nathan, G.J. and Mi, J. *Phys. Fluids*, submitted, 2001.